itive total dissipation $\mathscr{E} = \mathscr{E}_2 - \mathscr{E}_1$ (*13*).

In the limit $\beta \gg 1$, the speed of energy change is so high that switching may take place only at $W > 0$, but within a much larger interval of energies: $\Delta W \sim \beta^{1/2} k_B T$. The average energy dissipation for this (irreversible) process is of the same order, that is, much greater than $k_B T$ and independent of T: $\mathscr{E} = (\pi\beta/2)^{1/2} k_B T = (\pi e^2 \alpha / 2G)^{1/2}$. The results of numerical calculation of $\mathscr{E}$ for intermediate values of β are represented by the solid line in Fig. 3. Taking into account that at $p \ll 1$ the parameter $\tau = \Delta/\alpha$ may be considered as the duration of the switching process (Fig. 1C), we find that all our asymptotic results can be summarized as follows:

$$\mathscr{E}\tau = \frac{\hbar}{GR_Q} \times \begin{cases} 0.67 \ln(1/p) \text{ for } \delta,\beta \ll 1 \\ 1.97\, \beta^{-1/2} \ln(1/p) \text{ for } \delta \ll 1 \ll \beta \\ 2.78 \left[\ln \dfrac{1}{2p \ln(1/p)} \right]^{1/2} \text{ for } 1 \ll \delta,\beta \end{cases} \quad (7)$$

where $R_Q = \pi\hbar/2e^2 \approx 6.45$ kilohms is the quantum unit of resistance. Because the orthodox theory is valid only at $GR_Q \ll 1$, within this theory $\mathscr{E}\tau \gg \hbar$ for any switching speed.

Our results demonstrate that reversible computation for which the energy dissipation $\mathscr{E}$ per bit is much less than $k_B T$ may be implemented in a physical system with discrete states. However, the quantum bound for the product $\mathscr{E}\tau$ obtained within our concrete model is much greater than that obtained earlier for a system with a continuous degree of freedom (*9*). It is possible that the $\hbar$ limit for $\mathscr{E}\tau$ may be overcome in the case of islands with discrete spectra of electron energies (*14*).

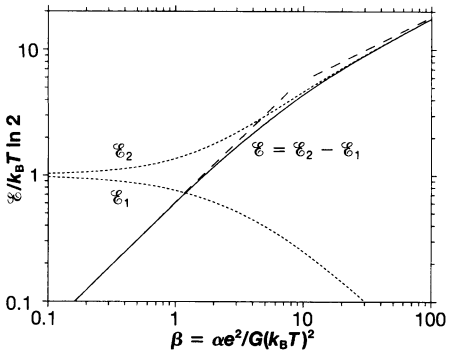

Fig. 3. Components of the energy exchange between the parametron and the heat bath as functions of the process speed $\alpha = dW/dt$. Short-dashed lines represent the average energy flow $\mathscr{E}_1$ from the heat bath to the parametron during the first half of the process ($W \le 0$) and the average flow $\mathscr{E}_2$ from the device back into the heat bath during its second half ($W \ge 0$), respectively. The solid line denotes the net energy dissipation $\mathscr{E} = \mathscr{E}_2 - \mathscr{E}_1$. The long-dashed line segments show the low-speed (adiabatic) and high-speed (diabatic) asymptotes of the function $\mathscr{E}(\alpha)$ (see equations in the text).

REFERENCES AND NOTES

1. K. K. Likharev, *IEEE Trans. Magn.* **13**, 242 (1976).
2. _____ and V. K. Semenov, *IEEE Trans. Appl. Supercond.* **1**, 3 (1991).
3. D. V. Averin and K. K. Likharev, in *Single Charge Tunneling*, H. Grabert and M. H. Devoret, Eds. (Plenum, New York, 1992), pp. 311–332.
4. A. N. Korotkov, *Appl. Phys. Lett.* **67**, 2412 (1995).
5. We consider only the case in which the state of the system can be described as a classical variable, in contrast to so-called "quantum computing devices" [for example, see I. L. Chuang, R. Laflamme, P. W. Shor, W. H. Zurek, *Science* **270**, 1633 (1995) and references therein]. These "classical" systems (whose dynamics may nevertheless require quantum-mechanical descriptions) may provide reliable computation even at substantial coupling to the environment.
6. This system was reinvented later as a "flux quantum parametron" [see K. F. Loe and E. Goto, *IEEE Trans. Magn.* **21**, 884 (1985)].
7. R. Landauer, *IBM J. Res. Dev.* **5**, 183 (1961); R. W. Keyes and R. Landauer, *ibid.* **14**, 152 (1970).
8. C. Bennett, *ibid.* **17**, 525 (1973).
9. K. K. Likharev, *Int. J. Theor. Phys.* **21**, 311 (1982).
10. _____ and A. N. Korotkov, in *Abstracts of the Fourth International Workshop on Computational Electronics*, Tempe, AZ, 30 October to 5 November 1995, p. 5.
11. D. V. Averin and K. K. Likharev, in *Mesoscopic Phenomena in Solids*, B. L. Altshuler, P. A. Lee, R. A. Webb, Eds. (Elsevier, Amsterdam, 1991), pp. 173–271.
12. A. N. Korotkov and K. K. Likharev, report presented at the *International Conference on Quantum Devices and Circuits*, Alexandria, Egypt, 4 to 8 June 1996.
13. Our discussion of entropy transfer serves only as an interpretation of our quantitative result for the energy dissipation, rather than its basis.
14. D. V. Averin and A. N. Korotkov, *J. Low Temp. Phys.* **80**, 173 (1990); M. Kastner, *Rev. Mod. Phys.* **64**, 849 (1992).

15. We thank D. V. Averin and T. Usuki for useful discussions. Supported in part by Office of Naval Research grant N00014-93-1-0880 and Air Force Office of Scientific Research grant F49620-95-1-0044.

29 February 1996; accepted 17 June 1996

"Tubules-Within-a-Tubule" Hierarchical Order of Mesoporous Molecular Sieves in MCM-41

Hong-Ping Lin and Chung-Yuan Mou*

The recently discovered mesoporous aluminosilicate MCM-41 consists of hexagonal arrays of nanometer-sized cylindrical pores. It is shown that this material can be synthesized by cooperative condensation of silicate and cylindrical cationic micelles. Careful control of the surfactant-water content and the rate of condensation of silica at high alkalinity resulted in hollow tubules 0.3 to 3 micrometers in diameter. The wall of the tubules consisted of coaxial cylindrical pores, nanometers in size, that are characteristic of those of MCM-41. The formation of this higher order structure may take place through a liquid crystal phase transformation mechanism involving an anisotropic membrane-to-tubule phase change. The hierarchical organization of this "tubules-within-a-tubule" particle texture is similar to that of the frustules of marine diatoms.

In the formation of mesoporous M41S family molecular sieves (*1*, *2*), cooperative formation of the surfactant phase is critical in determining the mesostructure (*2*, *3*). By varying the surfactant/silicate ratio, one can form hexagonal, cubic, or lamellar structures as the surfactant/silicate ratio increases (*2*, *4*). This is parallel to the known phase behavior in simple water/surfactant systems for cationic (*5*) and anionic (*6*) surfactants, where increasing surfactant concentration will usually make the following transformation: micellar solution L1 → hexagonal H1 → intermediate I → lamellar Lα (*5*). According to the balance of free energy between hydrophilic and hydrophobic groups, this transformation can also be brought about by decreasing the repulsion in the head group of the surfactant molecule (*6*).

For a complex mixture of surfactant and silicates, the liquid crystal structures formed are highly sensitive to the conditions of the solution. Various controllable factors, such as temperature, alkalinity, and the addition of counterions and alcohols, can induce mesoscopic structural change by modifying the rigidity and curvature of the interfaces (*7*–*11*). For the synthesis of MCM-41, when the structure is soft and before extensive polymerization of silicates, higher order organization may be thus controlled and formed. Here we report that solvent-separated multilayers of periodic hexagonal MCM-41 silicates can be formed and further bent into hollow microtubules (micrometer size) with the nanochannels forming the walls of these tubules. The resulting cylindrical silica has a hierarchical order of tubules within a tubule.

Surfactant and silicate were mixed in

Department of Chemistry, National Taiwan University, Taipei, Taiwan. E-mail: cymou@cc.ntu.edu.tw

*To whom correspondence should be addressed.

high alkalinity. Acidification was then accomplished by the slow addition of H_2SO_4. Thermally stable MCM-41 zeolites can be synthesized at room temperature in such a simple process (*12*). To prepare the aluminosilicate MCM-41, we dissolved 0.060 g of sodium aluminate (54% Al_2O_3; Riede-de Haën, Germany) in 3.0 g of water and mixed this with 30.0 g of a 12% C_{16}TMAB (cetyltrimethylammonium bromide, 99%; Merck) aqueous solution. Then 5.3 g of sodium silicate (27% SiO_2 and 14% NaOH; Aldrich) was added to the above solution. After the resulting mixture was stirred for 10 min at room temperature, 6.0 g of 1.1 M H_2SO_4 solution was added by pipette very slowly (total time ~30 min). (A fast rate of acidification results in the usual MCM-41 microparticles instead of the hollow tubule morphology reported here.) The pH of the final mixture was ~10.0. The gel mixture formed after this acidification was allowed to stand for 20 min and then was heated at 100°C for 48 hours in an autoclave. The solid product recovered by filtration was washed with deionized water, dried at ambient conditions, and calcined at 540°C in air for 6 hours to remove the template. The same experiment was also performed with pure silica (that is, without addition of sodium aluminate).

To investigate the process of morphological change of this MCM-41 material, we examined the products at various stages of the acidification by x-ray diffraction (XRD) pattern and scanning electron microscopy (SEM). Before addition of the H_2SO_4, the surfactant-aluminate-silicate mixture appeared to be an opaque white suspension. In the early stage of acidification, the mixture underwent a phase separation to form a surfactant-rich viscous gel phase and a clear aqueous solution. Further addition of acid led to a sudden dispersion and precipitation of the upper surfactant-rich layer. The XRD pattern of the as-synthesized material (sample A) at this early stage of neutralization (Fig. 1A) is typical for hexagonal MCM-41, with d_{100} = 4.0 nm (where d is the center-to-center distance of micelles in hexagonal packing). An SEM micrograph of sample A (Fig. 2A) shows, however, a layered lamellar-type structure, where at least six layers can be discerned. Subsequent addition of acid to the mixture resulted in another as-synthesized sample (sample B), in which the XRD pattern maintained the same hexagonal arrangement of MCM-41 with more distinct (110) and (200) peaks (Fig. 1B). The SEM micrograph of sample B shows that the layers in sample A broke up into microtubules (Fig. 2B). After complete addition of acid, the sample completely transformed into tubules with a rather uniform diameter (~0.3 μm) and average length (~5 μm).

After its hydrothermal reaction at 100°C, we obtained an XRD pattern and micrograph of the filtered sample C (Figs. 1C and 2C, respectively). The d spacing of sample C increased slightly to 4.16 nm, and the tubular structure was maintained. Enlargement of the image, showing some of the broken ends of the tubule, revealed that it is hollow. Calcination of sample C resulted in sample D, in which the SEM showed almost the same pattern as in sample C. Examining many of the SEM micrographs, we found that the tubular form represents >95% of the solid material. Its XRD pattern (Fig. 1D) indicates that it has a well-developed hexagonal MCM-41 structure with some shrinkage of d spacing to 3.96 nm. This very slight shrinkage after calcination indicates that the nanostructure is strong.

Transmission electron microscopy (TEM) of sample C (Fig. 3A) shows equidistant parallel lines, along the tubular axis, with an apparent average spacing at ~3.70 nm, which gives a distance of 4.27 nm after multiplication by the $2/\sqrt{3}$ geometry factor (*13*). This value is in reasonable agreement with the XRD result. From Fig. 3A, it is also

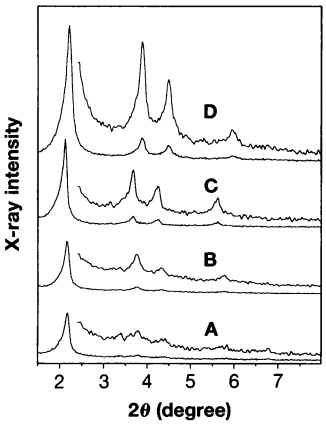

Fig. 1. Powder XRD patterns of mesostructure precipitated from the same mixture with the following mole ratio at various stages of synthesis: 1 Al_2O_3:75 SiO_2:30 Na_2O:35 CTAB:6244 H_2O. (**A**) Sample A, as synthesized at room temperature with H_2SO_4/Al_2O_3 = 5.7. (**B**) Sample B, as-synthesized at room temperature with H_2SO_4/Al_2O_3 = 17.0. (**C**) Sample C, after complete addition of acid (H_2SO_4/Al_2O_3 = 21.6) and hydrothermal reaction. (**D**) Sample D, after calcination of sample C. The patterns were measured on a Scintag X1 diffractometer with Cu Kα radiation (wavelength = 0.154 nm). The upper trace of each sample is five times that of the lower trace.

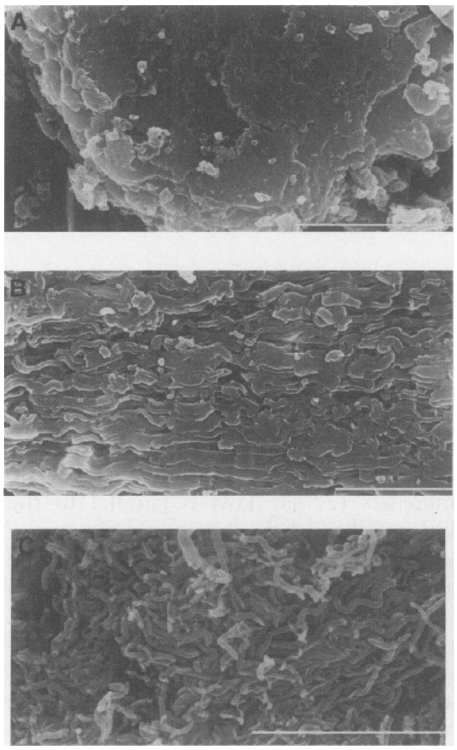

Fig. 2. Scanning electron micrographs showing the morphology at various stages of synthesis of aluminosilicate MCM-41 under the same conditions as in Fig. 1. (**A**) Sample A. (**B**) Sample B. (**C**) Sample C. The micrographs were taken on a Hitachi S-2400 microscope with an accelerating voltage of 20 kV.

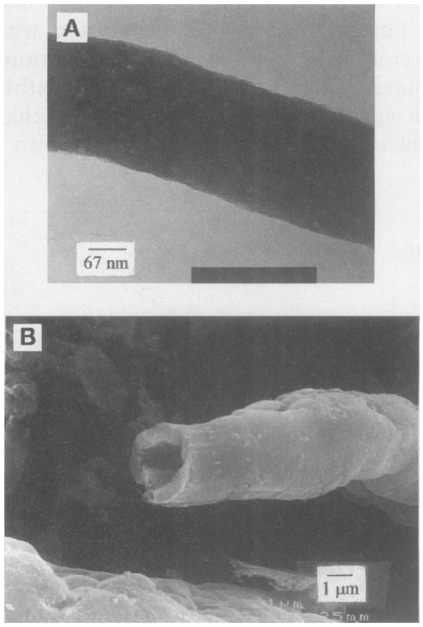

Fig. 3. (**A**) Transmission electron micrograph of the as-synthesized tubular aluminosilicate MCM-41 material before calcination to obtain sample C. The micrographs were taken on a Hitachi H-7100 microscope with an accelerating voltage of 100 kV. (**B**) Scanning electron micrograph of calcined product of tubular pure silica MCM-41. The micrograph was taken on a JEOL JSM-6300 microscope with an accelerating voltage of 20 kV.

apparent that the darkness of the parallel lines is not uniform, a defect that is probably due to broken channels.

The calcined product was further characterized by a N_2 adsorption-desorption isotherm, which gave a Brunaer-Emmett-Teller surface area of 1066 m^2 g^{-1}. The pore size distribution shows an average pore size of about 2.6 nm and half-height width of 0.2 nm. In addition to the sharp increase of volume adsorbed at $P/P_0 \approx 0.34$ (where P is pressure), there is a substantial hysteresis in the isotherm at $P/P_0 > 0.45$. This effect may be due to a packing defect in the formation of the tubules. The bending and closing-up process in a membrane-to-tubule translation will unavoidably create some stress, and thus packing defects, between the cylindrical micelles. ^{27}Al nuclear magnetic resonance (NMR) spectroscopy of the as-synthesized material showed a peak only at 52 parts per million (ppm), which indicates that all of the aluminum resides in the skeleton.

We have also performed the same synthesis procedure to prepare pure silica MCM-41 without any addition of alumina source. The calcined product also revealed a microtubular morphology, as shown by SEM (Fig. 3B), with a much larger outer diameter (~3 μm) and length (>20 μm). The microtubule is hollow, with a wall thickness ~0.6 μm; however, unlike the uniformity of aluminosilicate microtubules in Fig. 2, the size of the hollow tubules of pure silica MCM-41 is nonuniform and the material is a mixture of the tubular and microparticle forms of MCM-41.

Two experimental factors are crucial to the formation of hollow microtubules: the ratio of surfactant to water in the reactant and the delayed slow neutralization procedure. Although there is a large range of surfactant/water ratios that permits the formation of periodical hexagonal-phase MCM-41, the corresponding range of ratios for the formation of hollow microtubules is relatively small. If the C_{16}TMAB/water ratio is too low, the product has the usual microparticle morphology. The neutralization step should also be slow. The hollow tubule structure can thus be formed at high pH, before the substantial polymerization of silicates results in rigid, unbending structures.

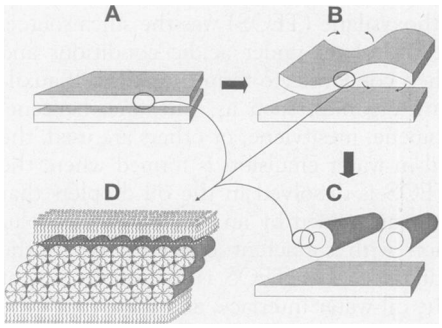

Fig. 4. Proposed mechanism for the formation of the microtubular morphology of MCM-41. (**A**) Mixed lamellar-hexagonal membrane phase. (**B**) Acidification leads to membrane curvature. (**C**) Neutralization bends the membrane into tubules. (**D**) The membrane consists of a hexagonal array of cylindrical micelles.

Given the almost complete transformation of the aluminosilicate at mild reaction conditions into the uniform size of hollow tubules, we propose a liquid crystal phase transformation mechanism for the formation of the new structure. In the beginning, under high pH, the silicate-surfactant system is close to the lamellar-hexagonal phase boundary. A little acidification results in a mixed lamellar-hexagonal phase in which layers of hexagonally arranged rod micelles are separated by bilayers of surfactants and water (Fig. 4A). This phase probably corresponds to the intermediate phase reported in the surfactant phase diagram (*5*). The layered structure can be stabilized by the electrostatic and entropic undulation repulsion force between the membrane layers (*14*).

Because the membrane layers are intrinsically anisotropic, further acidification leading to the condensation of silicates and charge imbalance on the membrane surface should favor the curvature of the membrane along only one direction (Fig. 4B), the transrod direction. Neutralization would then bend the membrane completely into tubules (Fig. 4C). A "natural wavelength" of destabilization can thus be expected and, as we observed, results in the formation of tubules with uniform diameters. The transformation of the lamellar → ripple → tubular phase is similar to the process in the formation of lipid tubules (*15*). Recently, multilamellar lipid tubules were observed through a first-order phase transition (*16*). It has been predicted that fluctuating tethered membranes with any intrinsic anisotropy unavoidably transform into "new" tubules (*17*), given enough driving force. In our case, the driving force arises from the charge imbalance at the surface, which is associated with the condensation reaction of the silicate-oxygen bond as the pH is lowered (*18*).

In the case of pure silica tubules, the membrane would be more thick and rigid and a ripple with a longer wavelength should be expected, as observed (*19*). As shown in Fig. 4A, we started with a mixed lamellar-hexagonal layer system, but a short-lived pure lamellar phase could also exist, as observed by Monnier *et al.* (*3*). In an experiment with the longer hydrocarbon chain octadecyltrimethylammonium bromide (C_{18}TMAB) replacing C_{16}TMAB, we captured an intermediate structure (from XRD) that is lamellar before it is transformed into the hexagonal phase (*20*). Therefore, the nanostructure of MCM-41 could also initially follow the lamellar mechanism proposed by Monnier (*3*) before forming the hexagonal phase and then follow the ripple → tubule transformation to form tubules.

The higher order hierarchical silica structures we synthesized have been extensively documented in the ultrastructure of the siliceous skeletons of marine diatoms and Radiolaria (*21*). In fact, the hollow tubular valve, with a large central area absent, of the diatom species *Annellus californicus* (*21*) looks similar to the hollow tubular structure we report here (*22*). The elaborate organization patterns in diatoms and Radiolaria are usually on the order of micrometers. Synthetic chemistry, in contrast, normally achieves self-organization patterns in the nanometer range. We have demonstrated that such higher order biomimetic self-organization can be accomplished in the laboratory. The liquid crystal phase transformation mechanism that we propose could provide a paradigm for understanding higher order biomineralization (*23*).

We have designed a strategy for producing hollow tubular forms of MCM-41 based on the sequential separation of self-organization of template silicates and the polymerization of silicates. By delaying the formation of the rigid structure, one can build the more complex tubules-within-a-tubule structure through a phase transformation of liquid crystal. This in turn may provide a way to explore the many complex structures that are possible in surfactant systems and to form zeolite structures. The ability to synthetically control the intricate hollow tubular form of the aluminosilicate MCM-41 could have applications in catalysis, separation technology, and opticoelectronics.

REFERENCES AND NOTES

1. C. T. Kresge, M. E. Leonowicz, W. J. Roth, J. C. Vartuli, J. S. Beck, *Nature* **359**, 710 (1992).
2. J. S. Beck *et al.*, *J. Am. Chem. Soc.* **114**, 10834 (1992).
3. A. Monnier *et al.*, *Science* **261**, 1299 (1993).
4. J. C. Vartuli *et al.*, *Chem. Mater.* **6**, 2317 (1994).
5. E. S. Blackmore and G. J. T. Tiddy, *J. Chem. Soc. Faraday Trans. II* **84** (no. 8), 1115 (1988).
6. A. Sein and J. B. F. N. Engberts, *Langmuir* **11**, 455 (1995).
7. M. Ogawa, *J. Am. Chem. Soc.* **116**, 7941 (1994).
8. P. T. Tanev and T. J. Pinnavaia, *Science* **271**, 1267 (1996).
9. S. Oliver, A. Kuperman, N. Coombs, A. Lough, G. A. Ozin, *Nature* **378**, 47 (1995).
10. A. Firouzi *et al.*, *Science* **267** 1138 (1995).
11. C. A. Fyfe and G. Fu, *J. Am. Chem. Soc.* **117**, 9709 (1995).
12. H. P. Lin, S. Cheng, C.-Y. Mou, unpublished results.
13. A. Chenite, Y. L. Page, A. Sayar, *Chem. Mater.* **7**, 1015 (1995).
14. W. Helfrich, *Z. Naturforsch.* **33a**, 305 (1978).
15. J. M. Schnur, *Science* **262,** 1669 (1993).
16. B. N. Thomas, C. R. Safinya, R. J. Plano, N. A. Clark, *ibid.* **267,** 1635 (1995).
17. L. Radzihovsky and J. Toner, *Phys. Rev. Lett.* **75**, 4752 (1995).
18. Although we did not capture a separate stable ripple

phase in our system, this ripple structure would provide a reasonable explanation of the intermediate structure observed in Fig. 2B. The ripple phase has been observed in many lipid systems (*24*) and can include macroripples with wavelengths of ~100 nm (*25*). The slow neutralization strategy is necessary to leave enough time for the soft layer containing the hexagonal phase to bend.

19. It has been reported by Z. Luan *et al.* [*J. Chem. Soc. Faraday Trans.* **91**, 2955 (1995)] that the crystal size of MCM-41 is reduced after incorporation of aluminum into the structure. In our case, this is reflected in shorter and thinner tubules when aluminum is incorporated into the framework.
20. H. P. Lin, S. Cheng, C.-Y. Mou, unpublished results.
21. L. H. Burekle, in *Introduction to Marine Micropaleontology*, B. U. Haq and A. Boersna, Eds. (Elsevier, New York, 1978), pp. 245–266.
22. The difference in pH between experimental conditions and the naturally occurring state of diatoms should be noted.
23. S. Mann, *J. Mater. Chem.* **5**, 935 (1995).
24. J. A. N. Zasadzinski, J. Schneir, J. Gurley, V. Elings, P. K. Hansma, *Science* **239**, 1013 (1988); D. C. Wack and W. W. Webb, *Phys. Rev. Lett.* **61**, 1210 (1988).
25. R. E. Brown, W. H. Anderson, V. S. Kulkarni, *Biophys. J.* **68**, 1396 (1995).
26. Supported by the National Science Council of Taiwan (NSC 85-2113-M-002-032cc). We thank S. Cheng and M.-P. Chen for valuable discussions.

2 April 1996; accepted 13 June 1996

Oil-Water Interface Templating of Mesoporous Macroscale Structures

S. Schacht, Q. Huo, I. G. Voigt-Martin, G. D. Stucky, F. Schüth*

Ordered mesostructured porous silicas that are also macroscopically structured were created by control of the interface on two different length scales simultaneously. Micellar arrays controlled the nanometer-scale assembly, and at the static boundary between an aqueous phase and an organic phase, control was achieved on the micrometer to centimeter scale. Acid-prepared mesostructures of silica were made with the *p*6, *Pm*3*n*, and the $P6_3/mmc$ structures in the form of porous fibers 50 to 1000 micrometers in length, hollow spheres with diameters of 1 to 100 micrometers, and thin sheets up to 10 centimeters in diameter and about 10 to 500 micrometers in thickness. These results might have implications for technical applications, such as slow drug-release systems or membranes, and in biomineralization, where many processes are also interface-controlled.

As noted by Israelachvili (*1*), microemulsions and emulsions occupy a special place in the hierarchy of structures, in that their formation involves long-range forces with an energy of assembly, including shape fluctuations and interaggregate interactions, approximately equal to the thermal energy kT. Hydrodynamic long-range forces can therefore be used to define emulsion morphology and the configuration of the emulsion oil-water interface. If an oil-in-water interface is used as an inorganic growth medium with the growth direction into the aqueous phase, morphological control of the resulting inorganic-organic composite assembly can be achieved at micrometer and longer length scales.

At a somewhat smaller length scale, mesoscale patterned silica-organic composite phases with organic domain dimensions of up to 0.01 μm and periodic repeats of as much as 0.02 μm (*2*) can now be created in a variety of two- and three-dimensional (2D and 3D) periodic arrays (*3–7*). These ordered organic-inorganic composite precursors of porous oxide structures form in a cooperative way under the influence of surfactants (*4–10*), with the nanophase dimensions and the overall 3D periodic geometries determined primarily by the surfactant molecular shape and geometry.

We combined long-range oil-in-water emulsion and oil-water interface physics with the shorter range cooperative assembly of silica and surfactants at the oil-water interface to create ordered composite mesostructured phases that are also macroscopically structured. The organic "oil" and surfactant can be removed from the silica phase to give mesoporous structures. Here the emulsion or the interface, or both, exerts morphological control during the formation of the inorganic gel or crystals.

With self-assembly energies approaching kT, emulsions are often close to the limit of stability. Oil-in-water emulsions are stabilized by short-range (10^{-7} m) and relatively weak van der Waals interactions between the hydrophobic tails of amphiphilic surfactants and the emulsion organic phase. The M41S silicate mesostructures first described by the Mobil group were synthesized with surfactants under alkaline conditions (pH 11 to 12). Under these basic conditions, composite formation is dominated by strong, direct interactions between positively charged surfactant (S^+) with negative inorganic silica solution species (I^-) and the consequent intermolecular interactions among the resulting molecular ion pairs (S^+I^-) (*9*). This interaction is energetically disadvantageous for the creation of silica composite macroscale structures by the process of "coating" surfactant molecules that are weakly coordinated to an organic surface through van der Waals interactions because if the surfactant molecules are abstracted from the organic media, macroscopic control of the product by the organic phase is lost.

An alternative synthetic approach is to use acid-prepared mesostructures (APMs) synthesized from very acidic solutions below the pH of the isoelectric point of silica (*5*). Under these conditions, halide ions (X^-) mediate the interaction between the surfactant and positively charged inorganic species ($S^+X^-I^+$) through weak hydrogen bonding forces so that the identity of the surfactant-coated organic surface is maintained (*11*). Silica mesostructured phases synthesized in this fashion have different composition, pore structure, and absorption properties compared with samples synthesized under alkaline conditions (*12*).

With this in mind, we exploited the biphase control in the synthesis of APMs on two different length scales simultaneously: synthesis at one scale forms the surfactant inorganic nanocomposite, and the other controls the secondary particle morphology on the micrometer to centimeter scale, with the large-scale control being similar to the approach of Walsh *et al.* (*13*). We used auxiliary organics to create an oil-in-water emulsion. In the acidic synthesis, tetraethoxysilane (TEOS) was the silica source. It hydrolyzes under acidic conditions and then condenses to form the APM. If auxiliary organics, such as *n*-hexane, benzene, toluene, mesitylene, or others are used, the oil-in-water emulsion is formed where the TEOS is dissolved in the oil droplets that are surrounded by an acidic aqueous solution with surfactant concentrated in the interface. The TEOS is hydrolyzed just at the oil-water interface, and there forms the mesostructure, which reflects on a larger length scale the size and shape of the oil spheres because the inorganic material solidifies around them.

A typical synthesis was carried out as follows: The surfactant [4.74 g of $C_{16}H_{33}N(CH_3)_3Br$ or similar molar amounts of

S. Schacht and F. Schüth, Institut für Anorganische Chemie, Johann Wolfgang Goethe Universität Frankfurt, Marie Curie Straße 11, 60439 Frankfurt, Germany.
Q. Huo and G. D. Stucky, Department of Chemistry, University of California, Santa Barbara, CA 93106, USA.
I. G. Voigt-Martin, Institut für Physikalische Chemie, Johannes Gutenberg-Universität Mainz, Welderweg 11, 55099 Mainz, Germany.

*To whom correspondence should be addressed.